

Maximum principle preserving and unconditionally stable scheme for a conservative Allen–Cahn equation

Yongho Choi^a, Junseok Kim^{b,*}

^a Department of Computer & Information Engineering, Daegu University, Gyeongsan-si, Gyeongsangbuk-do 38453, Republic of Korea

^b Department of Mathematics, Korea University, Seoul 02841, Republic of Korea

ARTICLE INFO

Keywords:

Maximum principle preserving
Conservative Allen–Cahn equation
Space–time dependent Lagrange multiplier

ABSTRACT

In this study, we present a novel conservative Allen–Cahn (CAC) equation and its maximum principle preserving and unconditionally stable numerical method. There have been many research works of the numerical methods for the CAC equation. To conserve the total mass, many mathematical models for the CAC equation introduced Lagrange multipliers which are added to the original Allen–Cahn equation. Therefore, some of the methods do not preserve the maximum principle, i.e., it is possible to have values greater than the maximum and smaller than the minimum values of the admissible solutions. In this study, we propose a novel CAC equation with a new Lagrange multiplier which is a power exponent to the concentration so that the maximum principle strictly holds. Furthermore, we describe the proposed numerical algorithm in detail and present several computational experiments to validate the superior performance of the proposed scheme.

1. Introduction

In this study, we present a maximum principle preserving and unconditionally stable numerical scheme for the following conservative Allen–Cahn (CAC) equation:

$$\frac{\partial \phi(\mathbf{x}, t)}{\partial t} = -\frac{F'(\phi(\mathbf{x}, t))}{\epsilon^2} + \Delta \phi(\mathbf{x}, t) + \alpha[\phi^{\beta(t)}(\mathbf{x}, t) - \phi(\mathbf{x}, t)], \quad (1)$$

$$\mathbf{x} \in \Omega, t > 0,$$

$$\mathbf{n} \cdot \nabla \phi(\mathbf{x}, t) = 0, \quad \mathbf{x} \in \partial \Omega, \quad (2)$$

where α is parameter and $\beta(t) > 0$ is a time-dependent Lagrange multiplier which makes the solution satisfy the mass conservative constraint. Here, $\Omega \subset \mathbf{R}^2$ or \mathbf{R}^3 , \mathbf{x} is the space variable, t is the time variable, and \mathbf{n} is the normal vector on $\partial \Omega$. The phase field function $\phi(\mathbf{x}, t)$ is the concentration of one component of the binary mixture at space \mathbf{x} and time t ; and satisfies a maximum principle, $0 \leq \phi(\mathbf{x}, t) \leq 1$. Furthermore, $F(\phi) = 0.25\phi^2(\phi - 1)^2$ is a double-well potential (see Fig. 1) and ϵ is a small interfacial parameter. When we consider excluding the α term, it becomes the Allen–Cahn (AC) equation:

$$\frac{\partial \phi(\mathbf{x}, t)}{\partial t} = -\frac{F'(\phi(\mathbf{x}, t))}{\epsilon^2} + \Delta \phi(\mathbf{x}, t). \quad (3)$$

The AC equation is the L_2 -gradient flow of the Ginzburg–Landau free energy functional:

$$\mathcal{E} = \int_{\Omega} \left(\frac{F(\phi)}{\epsilon^2} + \frac{1}{2} |\nabla \phi|^2 \right) dx. \quad (4)$$

When Eq. (4) is differentiated with respect to time t , its temporal derivative is not positive, therefore, the total energy decreases with time. The AC equation is an equation derived from a study on phase separation of Fe–Al alloys [1], and various studies have been done such as time-dependent AC equation on surfaces with radial basis functions [2], discrete maximum principle and energy stability scheme [3], high order structure preserving algorithm with a nonlocal constraint [4], maximum principle preserving scheme with local discontinuous Galerkin methods [5], high order compact structure preserving difference scheme [6], and explicit stable method using alternating direction explicit method for the diffusion term [7].

Recently, the CAC equation has been used in many applications such as two-phase fluid flows [8–10], multiphase fluid flows [11–13], solving PDE on surfaces [14,15], diblock copolymers [16]. To conserve a mass, the authors [17] introduced a time dependent Lagrange multiplier $\beta(t)$

$$\frac{\partial \phi(\mathbf{x}, t)}{\partial t} = -\frac{F'(\phi(\mathbf{x}, t))}{\epsilon^2} + \Delta \phi(\mathbf{x}, t) + \beta(t), \quad (5)$$

where $\beta(t)$ is given as $\beta(t) = \int_{\Omega} F'(\phi(\mathbf{x}, t)) dx / (\epsilon^2 \int_{\Omega} dx)$ to keep the mass conservation and this formulation has been widely used [18–21]. The authors in [22] presented the following CAC equation:

$$\frac{\partial \phi(\mathbf{x}, t)}{\partial t} = -\frac{F'(\phi(\mathbf{x}, t))}{\epsilon^2} + \Delta \phi(\mathbf{x}, t) + \beta(t) \sqrt{2F(\phi(\mathbf{x}, t))}, \quad (6)$$

* Corresponding author.

E-mail addresses: yongho_choi@daegu.ac.kr (Y. Choi), cfdkim@korea.ac.kr (J. Kim).

URLs: <https://sites.google.com/view/yh-choi> (Y. Choi), <https://mathematicians.korea.ac.kr/cfdkim> (J. Kim).

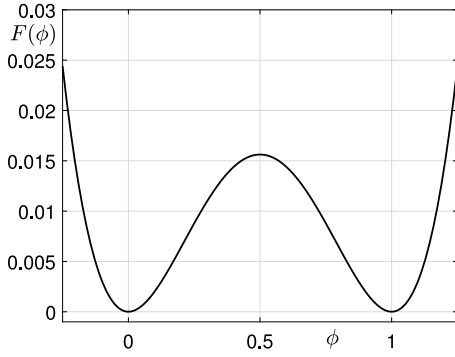


Fig. 1. Double-well potential free energy function, $F(\phi) = \phi^2(\phi - 1)^2/4$ which has the global minimum value at $\phi = 0$ and $\phi = 1$.

where $\beta(t) = \int_{\Omega} F'(\phi(\mathbf{x}, t))d\mathbf{x} / [\epsilon^2 \int_{\Omega} \sqrt{2F(\phi(\mathbf{x}, t))}d\mathbf{x}]$ and $F(\phi) = 0.25\phi^2(\phi - 1)^2$. This type of the CAC Eq. (6) has been widely used in various researches [23–26]. Recently, the CAC equation with a curvature-dependent Lagrange multiplier was developed in [27]. The above-mentioned AC and CAC equations are included in category of the phase field model. More phase field models are the Cahn–Hilliard equation, phase field crystal equation, etc., and various related studies have been conducted [28–35].

In this study, we use the following definition of the maximum principle: If $0 \leq \phi(\mathbf{x}, 0) \leq 1$, then $0 \leq \phi(\mathbf{x}, t) \leq 1$ is satisfied for all time t , where $\phi(\mathbf{x}, t)$ is the solution of the CAC equation. Strictly speaking, our proposed method is a maximum bound principle preserving method [36]. That is, the phase-field value can be larger than the maximum of the given initial values; however, its values are in the bounded range. Unlike the previous CAC Eqs. (5) and (6), the proposed CAC equation allows a numerical scheme which preserves the maximum principle.

However, most of the previous mathematical models and numerical methods do not satisfy strict discrete maximum principle mainly due to the way of mass correction step. Mass corrections are done by addition or subtraction to the phase-field function. Therefore, it may violate the discrete maximum principle, i.e., the phase-field function can have values less than zero or greater than one, which is non-physical value.

There have some research works to resolve the violation problem of the maximum principle. In [8], the authors developed a consistent and conservative boundedness mapping algorithm. In [37], the authors presented improved stabilized integrating factor Runge–Kutta (RK) methods for the CAC equations. The presented methods preserve the maximum principle unconditionally and conserve the mass to machine accuracy.

To overcome this drawback, in this study we propose a new simple mass correction step which takes a positive power to the phase-field function whose range is from zero to one.

The contents of this paper is as follows. In Section 2, the proposed computational method is described. In Section 3, the numerical results are presented. In Section 4, we conclude.

2. Description of the numerical scheme

Now, we present the description of the maximum principle preserving and unconditionally stable numerical scheme for the proposed CAC equation. Using the operator splitting technique [38–40]. Recently, there are also theoretical studies on the stability and convergence of the operator splitting method for the AC equation [41,42]. We split Eq. (2) as follows:

$$\frac{\partial \phi(\mathbf{x}, t)}{\partial t} = \Delta \phi(\mathbf{x}, t), \tag{7}$$

$$\frac{\partial \phi(\mathbf{x}, t)}{\partial t} = -\frac{F'(\phi(\mathbf{x}, t))}{\epsilon^2}, \tag{8}$$

$$\frac{\partial \phi(\mathbf{x}, t)}{\partial t} = \alpha[\phi^{\beta(t)}(\mathbf{x}, t) - \phi(\mathbf{x}, t)]. \tag{9}$$

We consider a two-dimensional domain, $\Omega = (L_x, R_x) \times (L_y, R_y)$. The three-dimensional (3D) numerical method is defined similarly and is a straightforward extension of the two-dimensional case. Therefore, we omit the details of the 3D extension for simplicity of exposition. However, we will present the 3D computational experiments for completeness. Let us discretize Ω as $\Omega_d = \{(x_i, y_j) | x_i = L_x + (i - 0.5)h, i = 1, \dots, N_x, y_j = L_y + (j - 0.5)h, j = 1, \dots, N_y\}$, where $h = (R_x - L_x)/N_x$ with integers N_x and N_y . We denote $\phi(x_i, y_j, n\Delta t)$ by ϕ_{ij}^n , where Δt is the time step. Note that, because Eq. (7) is a partial differential equation (PDE), we use the zero Neumann boundary condition to solve it. However, because Eqs. (8) and (9) are of the ordinary differential equation type, no spatial boundary conditions are needed.

In this study, we use the following definition of the discrete maximum principle: If $0 \leq \phi_{ij}^0 \leq 1$, then $0 \leq \phi_{ij}^n \leq 1$ is satisfied for all time step n , where ϕ_{ij}^n is the numerical solution of the discrete CAC equation. For given ϕ_{ij}^n for $i = 1, \dots, N_x$ and $j = 1, \dots, N_y$, we apply the operator splitting method and first solve the diffusion term, Eq. (7).

$$\frac{\phi_{ij}^{n+1,1} - \phi_{ij}^n}{\Delta t} = \Delta_d \phi_{ij}^{n+1,1}. \tag{10}$$

We use the finite difference method (FDM) for the x -directional term:

$$\frac{\phi_{ij}^{n+1,1} - \phi_{ij}^n}{\Delta t} = \Delta_d^x \phi_{ij}^{n+1,1} = \frac{\phi_{i+1,j}^{n+1,1} - 2\phi_{ij}^{n+1,1} + \phi_{i-1,j}^{n+1,1}}{h^2}, \tag{11}$$

which is solved by using the Thomas algorithm for the tri-diagonal system [43] with the zero Neumann boundary condition, i.e., $\phi_{0j}^{n+1,1} = \phi_{1j}^{n+1,1}$ and $\phi_{N_x+1,j}^{n+1,1} = \phi_{N_x,j}^{n+1,1}$ for $j = 1, \dots, N_y$. The zero Neumann boundary condition means 90° contact angle condition [44]. Similarly, we use the FDM for the y -directional term:

$$\frac{\phi_{ij}^{n+1,2} - \phi_{ij}^{n+1,1}}{\Delta t} = \Delta_d^y \phi_{ij}^{n+1,2} = \frac{\phi_{i,j+1}^{n+1,2} - 2\phi_{ij}^{n+1,2} + \phi_{i,j-1}^{n+1,2}}{h^2} \tag{12}$$

with $\phi_{i0}^{n+1,2} = \phi_{i1}^{n+1,2}$ and $\phi_{i,N_y+1}^{n+1,2} = \phi_{i,N_y}^{n+1,2}$ for $i = 1, \dots, N_x$.

Second, we analytically solve Eq. (8) using separation of variables [25]:

$$\phi_{ij}^{n+1,3} = 0.5 - \frac{1 - 2\phi_{ij}^{n+1,2}}{2\sqrt{(1 - 2\phi_{ij}^{n+1,2})^2 + 4\phi_{ij}^{n+1,2}(1 - \phi_{ij}^{n+1,2})}e^{-\frac{\Delta t}{2\epsilon^2}}}. \tag{13}$$

Finally, we numerically solve Eq. (9) using an explicit Euler method:

$$\frac{\phi_{ij}^{n+1} - \phi_{ij}^{n+1,3}}{\Delta t} = \alpha[(\phi_{ij}^{n+1,3})^{\beta^n} - \phi_{ij}^{n+1,3}], \tag{14}$$

where β^n is chosen to satisfy the conservation of the total mass, i.e.,

$$\sum_{i=1}^{N_x} \sum_{j=1}^{N_y} \phi_{ij}^{n+1} = \sum_{i=1}^{N_x} \sum_{j=1}^{N_y} \phi_{ij}^0. \tag{15}$$

To find β^n , we let $\alpha = 1/\Delta t$, then Eq. (14) becomes

$$\phi_{ij}^{n+1} = (\phi_{ij}^{n+1,3})^{\beta^n}. \tag{16}$$

From Eq. (15) and (16), we have

$$\sum_{i=1}^{N_x} \sum_{j=1}^{N_y} (\phi_{ij}^{n+1,3})^{\beta^n} = \sum_{i=1}^{N_x} \sum_{j=1}^{N_y} \phi_{ij}^0. \tag{17}$$

As schematically illustrated in Fig. 2, if $\beta^n < 1$, then $\sum_{i=1}^{N_x} \sum_{j=1}^{N_y} (\phi_{ij}^{n+1,3})^{\beta^n}$ in Eq. (17) becomes larger than $\sum_{i=1}^{N_x} \sum_{j=1}^{N_y} \phi_{ij}^{n+1,3}$. If $\beta^n > 1$, then $\sum_{i=1}^{N_x} \sum_{j=1}^{N_y} (\phi_{ij}^{n+1,3})^{\beta^n}$ in Eq. (17) becomes smaller than $\sum_{i=1}^{N_x} \sum_{j=1}^{N_y} \phi_{ij}^{n+1,3}$. Therefore, we can find an appropriate β^n value which satisfies

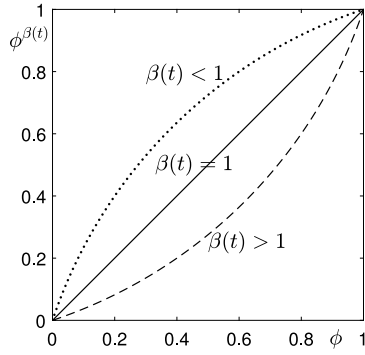


Fig. 2. Schematic illustration of $\phi^{\beta(t)}$ against ϕ . In practice, the value of $\beta(t)$ is very close to 1.

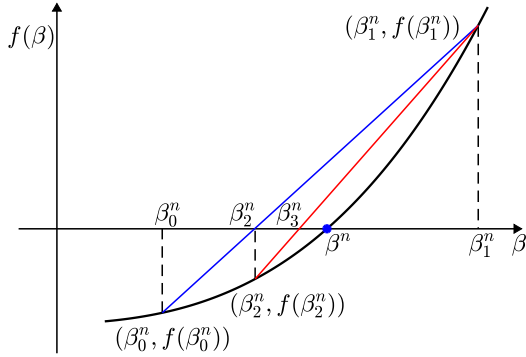


Fig. 3. Schematic illustration of the Secant method for finding the root β^n of $f(\beta)$, i.e., $f(\beta^n) = 0$.

Eq. (16). Because Eq. (17) is a highly nonlinear equation, we solve it using the Secant method [45]. Let

$$f(\beta) = \sum_{i=1}^{N_x} \sum_{j=1}^{N_y} \phi_{ij}^0 - \sum_{i=1}^{N_x} \sum_{j=1}^{N_y} (\phi_{ij}^{n+1,3})^\beta. \quad (18)$$

We start generating the sequence of approximations using the Secant method by setting $\beta_0^n < 1 < \beta_1^n$. In this study, we set $\beta_0^n = 0.98$ and $\beta_1^n = 1.02$. Then, the Secant method is as follows:

$$\beta_{k+1}^n = \beta_k^n - \frac{f(\beta_k^n)(\beta_k^n - \beta_{k-1}^n)}{f(\beta_k^n) - f(\beta_{k-1}^n)}, \text{ for } k = 1, \dots \quad (19)$$

As schematically illustrated in Fig. 3, starting with the two given values β_0^n and β_1^n , the value β_2^n is the intercept of the horizontal axis and line joining $(\beta_0^n, f(\beta_0^n))$ and $(\beta_1^n, f(\beta_1^n))$. The value β_3^n is the intercept of the horizontal axis and line joining $(\beta_1^n, f(\beta_1^n))$ and $(\beta_2^n, f(\beta_2^n))$, and so on. We can observe that the sequence $\{\beta_i^n\}_{i=0}^\infty$ converges to the root β^n of $f(\beta)$, i.e., $f(\beta^n) = 0$.

We use a stopping condition in the Secant method based on the consecutive difference, $|f(\beta_k^n) - f(\beta_{k-1}^n)| < tol$, where tol is a given tolerance. If that stopping condition is satisfied, then we let $\beta^n = \beta_k^n$. Finally, we obtain the updated numerical solution ϕ_{ij}^{n+1} from Eq. (16) using β^n .

We also numerically solve Eqs. (5) and (6) using operator splitting method: In both equations, the diffusion term is solved first by the implicit Euler method, and then the reaction term is calculated directly using the closed-form solution as in the previous research [25].

$$\frac{\phi_{ij}^{n+1,1} - \phi_{ij}^n}{\Delta t} = \Delta_d \phi_{ij}^{n+1,1}, \quad (20)$$

$$\phi_{ij}^{n+1,2} = 0.5 - \frac{1 - 2\phi_{ij}^{n+1,1}}{2\sqrt{(1 - 2\phi_{ij}^{n+1,1})^2 + 4\phi_{ij}^{n+1,1}(1 - \phi_{ij}^{n+1,1})}} e^{-\frac{\Delta t}{2\epsilon^2}}. \quad (21)$$

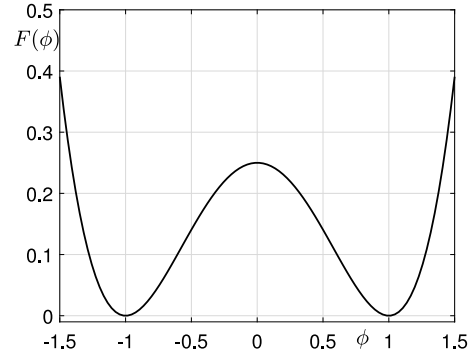


Fig. 4. Double-well free energy density function, $F(\phi) = 0.25(\phi^2 - 1)^2$ which has the global minimum value at $\phi = -1$ and $\phi = 1$.

After that, we solve the mass conservation term for Eq. (5) as Eq. (22)

$$\frac{\phi_{ij}^{n+1} - \phi_{ij}^{n+1,2}}{\Delta t} = \beta^{n+1,2}, \quad (22)$$

where $\beta^{n+1,2} = \frac{1}{\Delta t} \sum_{i=1}^{N_x} \sum_{j=1}^{N_y} (\phi_{ij}^0 - \phi_{ij}^{n+1,2})$, and for Eq. (6) as Eq. (23)

$$\frac{\phi_{ij}^{n+1} - \phi_{ij}^{n+1,2}}{\Delta t} = \beta^{n+1,2} \sqrt{2F(\phi_{ij}^{n+1,2})}, \quad (23)$$

where $\beta^{n+1,2} = \frac{1}{\Delta t} \sum_{i=1}^{N_x} \sum_{j=1}^{N_y} (\phi_{ij}^0 - \phi_{ij}^{n+1,2}) / \sum_{i=1}^{N_x} \sum_{j=1}^{N_y} \sqrt{2F(\phi_{ij}^{n+1,2})}$.

Theorem 1. The proposed numerical method (10)–(14) for the CAC model (2) satisfies the discrete maximum principle.

Proof. We note that $0 \leq \phi_{ij}^{n+1} \leq 1$ is always satisfied if $0 \leq \phi_{ij}^{n+1,3} \leq 1$ for any $\beta^n \geq 0$ by the definition Eq. (16). This fact is the key element in the following proof.

Let us assume $0 \leq \phi_{ij}^n \leq 1$ and we want to show $0 \leq \phi_{ij}^{n+1} \leq 1$, which implies the proposed method satisfies the discrete maximum principle. In the first step, it is well known that the fully implicit Euler schemes (Eqs. (11) and (12)) satisfy the discrete maximum principle, therefore, $0 \leq \phi_{ij}^{n+1,1} \leq 1$ and $0 \leq \phi_{ij}^{n+1,2} \leq 1$ hold. In the second step, $\phi_{ij}^{n+1,3}$ in Eq. (13) is bounded by 0 and 1 for $i = 1, \dots, N_x$ and $j = 1, \dots, N_y$, i.e., $0 \leq \phi_{ij}^{n+1,3} \leq 1$. In the third step, because of the non-negativity of β^n and $0 \leq \phi_{ij}^{n+1,3} \leq 1$, therefore, $0 \leq \phi_{ij}^{n+1} \leq 1$ is satisfied. Hence, the proof of the discrete maximum principle of the proposed method is complete. In addition, this result holds for arbitrary time step sizes. Therefore, the proposed numerical method is unconditionally stable. \square

We note that there is another popular quartic polynomial free energy function, $F(\phi) = 0.25(\phi^2 - 1)^2$, which is frequently used in literature. It has minimum at $\phi = -1$ and $\phi = 1$. If this free energy potential is used, then the governing CAC equation becomes

$$\begin{aligned} \frac{\partial \phi(\mathbf{x}, t)}{\partial t} &= -\frac{F'(\phi(\mathbf{x}, t))}{\epsilon^2} + \Delta \phi(\mathbf{x}, t) \\ &+ \alpha \left[\left(\frac{\phi(\mathbf{x}, t) + 1}{2} \right)^{\beta(t)} - \left(\frac{\phi(\mathbf{x}, t) - 1}{2} \right)^{\beta(t)} \right]. \end{aligned} \quad (24)$$

We briefly present the maximum principle preserving and unconditionally stable numerical method for the proposed CAC equation with another quartic polynomial free energy function, $F(\phi) = (\phi^2 - 1)^2/4$, see Fig. 4.

Using the operator splitting technique, we split Eq. (24) as follows:

$$\frac{\partial \phi(\mathbf{x}, t)}{\partial t} = \Delta \phi(\mathbf{x}, t), \quad (25)$$

$$\frac{\partial \phi(\mathbf{x}, t)}{\partial t} = -\frac{F'(\phi(\mathbf{x}, t))}{\epsilon^2}, \quad (26)$$

$$\frac{\partial \phi(\mathbf{x}, t)}{\partial t} = \alpha \left[\left(\frac{\phi(\mathbf{x}, t) + 1}{2} \right)^{\beta(t)} - \left(\frac{\phi(\mathbf{x}, t) - 1}{2} \right)^{\beta(t)} \right]. \quad (27)$$

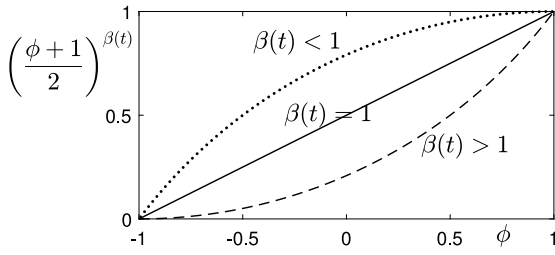


Fig. 5. Schematic illustration of $(0.5\phi(x,t) + 0.5)^{\beta(t)}$ against ϕ . In practice, the value of $\beta(t)$ is very close to 1.

For given ϕ_{ij}^n for $i = 1, \dots, N_x$ and $j = 1, \dots, N_y$, we apply the operator splitting method for the space derivatives in Eq. (25). We use FDM for the x - and y -directional terms:

$$\frac{\phi_{ij}^{n+1,1} - \phi_{ij}^n}{\Delta t} = \Delta_x^x \phi_{ij}^{n+1,1} \quad \text{and} \quad \frac{\phi_{ij}^{n+1,2} - \phi_{ij}^{n+1,1}}{\Delta t} = \Delta_y^y \phi_{ij}^{n+1,2}, \quad (28)$$

where we use the homogeneous Neumann boundary condition. Second, we analytically solve Eq. (26) using separation of variables [39]:

$$\phi_{ij}^{n+1,3} = \frac{\phi_{ij}^{n+1,2}}{\sqrt{(\phi_{ij}^{n+1,2})^2 + (1 - (\phi_{ij}^{n+1,2})^2) e^{-\frac{2\Delta t}{\epsilon^2}}}}. \quad (29)$$

Finally, we solve Eq. (27) using an explicit Euler-type method:

$$\frac{\phi_{ij}^{n+1} - \phi_{ij}^{n+1,3}}{\Delta t} = \alpha \left[\left(\frac{\phi_{ij}^{n+1,3} + 1}{2} \right)^{\beta^n} - \left(\frac{\phi_{ij}^{n+1,3} + 1}{2} \right) \right], \quad (30)$$

where β^n is chosen to satisfy the conservation of the total mass, i.e.,

$$\sum_{i=1}^{N_x} \sum_{j=1}^{N_y} \phi_{ij}^{n+1} = \sum_{i=1}^{N_x} \sum_{j=1}^{N_y} \phi_{ij}^0. \quad (31)$$

To find β^n , we rewrite Eq. (30) as

$$\frac{(\phi_{ij}^{n+1} + 1)/2 - (\phi_{ij}^{n+1,3} + 1)/2}{\Delta t/2} = \alpha \left[\left(\frac{\phi_{ij}^{n+1,3} + 1}{2} \right)^{\beta^n} - \left(\frac{\phi_{ij}^{n+1,3} + 1}{2} \right) \right] \quad (32)$$

and let $\alpha = 2/\Delta t$, then Eq. (32) becomes

$$\frac{\phi_{ij}^{n+1} + 1}{2} = \left(\frac{\phi_{ij}^{n+1,3} + 1}{2} \right)^{\beta^n}. \quad (33)$$

From Eqs. (31) and (33), we have

$$\sum_{i=1}^{N_x} \sum_{j=1}^{N_y} \left(\frac{\phi_{ij}^{n+1,3} + 1}{2} \right)^{\beta^n} = \sum_{i=1}^{N_x} \sum_{j=1}^{N_y} \frac{\phi_{ij}^0 + 1}{2}. \quad (34)$$

We solve Eq. (34) using the Secant method and Fig. 5 shows schematic illustration of $(0.5\phi(x,t) + 0.5)^{\beta(t)}$ against ϕ .

Finally, we obtain the updated numerical solution ϕ_{ij}^{n+1} from Eq. (33) with β^n , i.e.,

$$\phi_{ij}^{n+1} = 2 \left(\frac{\phi_{ij}^{n+1,3} + 1}{2} \right)^{\beta^n} - 1. \quad (35)$$

Furthermore, we consider the case of the CAC equation with logarithmic Flory–Huggins potential energy function (36),

$$F(\phi) = \frac{\theta}{2} [(1 + \phi) \ln(1 + \phi) + (1 - \phi) \ln(1 - \phi)] - \frac{\theta_c}{2} \phi^2, \quad (36)$$

where θ and θ_c are two positive constants satisfying $\theta \leq \theta_c$ [46]. If this logarithmic potential energy is used, then the governing CAC equation

becomes

$$\frac{\partial \phi(\mathbf{x}, t)}{\partial t} = -\frac{F'(\phi(\mathbf{x}, t))}{\epsilon^2} + \Delta \phi(\mathbf{x}, t) + \alpha \left[\left(\frac{\phi(\mathbf{x}, t) - \phi_\alpha}{\phi_\beta - \phi_\alpha} \right)^{\gamma(t)} - \left(\frac{\phi(\mathbf{x}, t) - \phi_\alpha}{\phi_\beta - \phi_\alpha} \right) \right], \quad (37)$$

where ϕ_α and ϕ_β are the two critical values of $F(\phi)$ defined in Eq. (36) [47]. Using the operator splitting technique, we split Eq. (37) as

$$\frac{\partial \phi(\mathbf{x}, t)}{\partial t} = \Delta \phi(\mathbf{x}, t), \quad (38)$$

$$\frac{\partial \phi(\mathbf{x}, t)}{\partial t} = -\frac{F'(\phi(\mathbf{x}, t))}{\epsilon^2}, \quad (39)$$

$$\frac{\partial \phi(\mathbf{x}, t)}{\partial t} = \alpha \left[\left(\frac{\phi(\mathbf{x}, t) - \phi_\alpha}{\phi_\beta - \phi_\alpha} \right)^{\gamma(t)} - \left(\frac{\phi(\mathbf{x}, t) - \phi_\alpha}{\phi_\beta - \phi_\alpha} \right) \right]. \quad (40)$$

Eq. (38) can be solved similarly to the previous method (28) and (39) can be solved using the interpolation method [47]. Then, we solve Eq. (40) using the explicit Euler-type method:

$$\frac{\phi_{ij}^{n+1} - \phi_{ij}^{n+1,3}}{\Delta t} = \alpha \left[\left(\frac{\phi_{ij}^{n+1,3} - \phi_\alpha}{\phi_\beta - \phi_\alpha} \right)^{\gamma^n} - \left(\frac{\phi_{ij}^{n+1,3} - \phi_\alpha}{\phi_\beta - \phi_\alpha} \right) \right], \quad (41)$$

where γ^n is chosen to satisfy the conservation of the total mass $\sum_{i=1}^{N_x} \sum_{j=1}^{N_y} \phi_{ij}^{n+1} = \sum_{i=1}^{N_x} \sum_{j=1}^{N_y} \phi_{ij}^0$. To find γ^n , we rewrite Eq. (41):

$$\frac{(\phi_{ij}^{n+1} - \phi_\alpha)/(\phi_\beta - \phi_\alpha) - (\phi_{ij}^{n+1,3} - \phi_\alpha)/(\phi_\beta - \phi_\alpha)}{\Delta t/(\phi_\beta - \phi_\alpha)} = \alpha \left[\left(\frac{\phi_{ij}^{n+1,3} - \phi_\alpha}{\phi_\beta - \phi_\alpha} \right)^{\gamma^n} - \left(\frac{\phi_{ij}^{n+1,3} - \phi_\alpha}{\phi_\beta - \phi_\alpha} \right) \right], \quad (42)$$

and let $\alpha = (\phi_\beta - \phi_\alpha)/\Delta t$, then Eq. (42) becomes

$$\frac{\phi_{ij}^{n+1} - \phi_\alpha}{\phi_\beta - \phi_\alpha} = \left(\frac{\phi_{ij}^{n+1,3} - \phi_\alpha}{\phi_\beta - \phi_\alpha} \right)^{\gamma^n}. \quad (43)$$

Then, we have

$$\sum_{i=1}^{N_x} \sum_{j=1}^{N_y} \left(\frac{\phi_{ij}^{n+1,3} - \phi_\alpha}{\phi_\beta - \phi_\alpha} \right)^{\gamma^n} = \sum_{i=1}^{N_x} \sum_{j=1}^{N_y} \frac{\phi_{ij}^0 - \phi_\alpha}{\phi_\beta - \phi_\alpha}. \quad (44)$$

We solve Eq. (44) using the Secant method. Finally, we obtain the updated numerical solution ϕ_{ij}^{n+1} from Eq. (43) with γ^n ,

$$\phi_{ij}^{n+1} = (\phi_\beta - \phi_\alpha) \left(\frac{\phi_{ij}^{n+1,3} - \phi_\alpha}{\phi_\beta - \phi_\alpha} \right)^{\gamma^n} + \phi_\alpha. \quad (45)$$

3. Numerical results

In this section, we simulate the comparison of results with previous models in two and three dimensions, the evolution of the circles, and numerical experiments to verify that the maximal principle and unconditional stability are satisfied. We shall use the thickness of transition layer $\epsilon_{9,5} \approx 0.0089$ if not otherwise specified, which is defined as $\epsilon_m = hm/[4\sqrt{2} \tanh^{-1}(0.9)]$ [48] and the time step $\Delta t = 1.0e-5$. We will denote the previous model1 (Eq. (5)) as PM1, the previous model2 (Eq. (6)) as PM2, and our proposed model (Eq. (2)) as PM3.

3.1. Comparison of three models

We perform the following numerical simulations to check the differences between PM1, PM2, and PM3. We use computational domain $\Omega = [0, 1]^2$ and mesh grid 128^2 . We define the initial conditions (1)

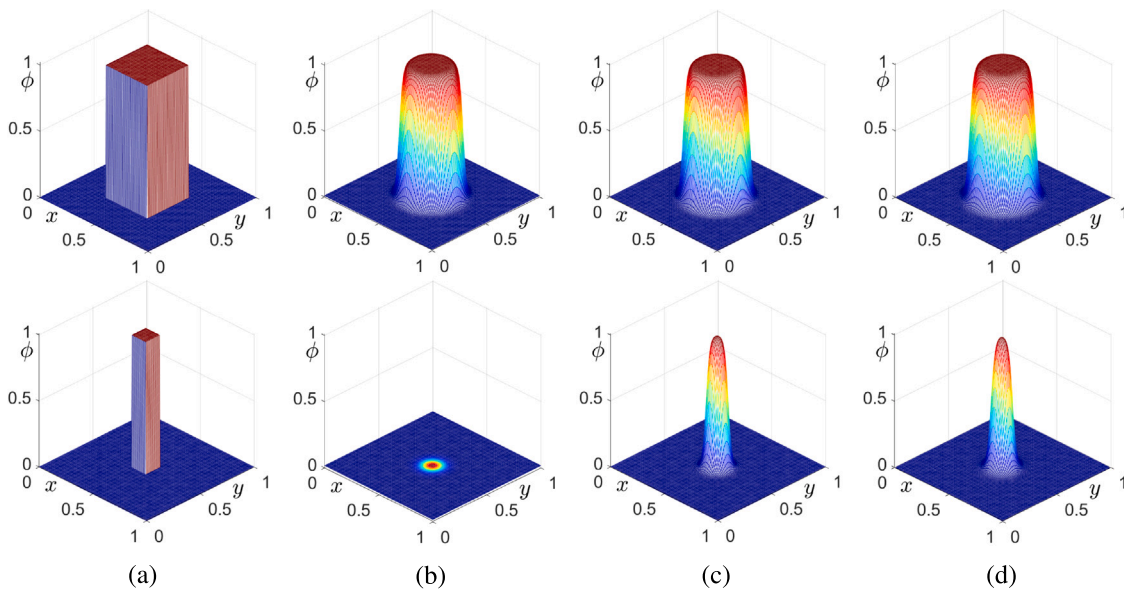


Fig. 6. (a): Two different sizes square shape initial conditions. (b)–(d): The numerical results at steady state of PM1, PM2, and PM3, respectively.

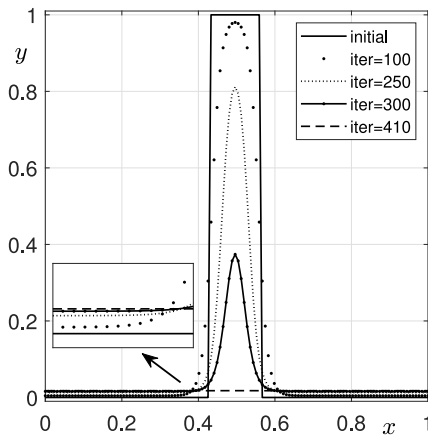


Fig. 7. Change of interface over time of PM1 when it has a small object as an initial condition.

when $40 \leq i, j \leq 88$, the value of ϕ_{ij} is 1, (2) when $56 \leq i, j \leq 72$, the value of ϕ_{ij} is 1, and otherwise the value of ϕ_{ij} is 0 (see Fig. 6(a)).

Figs. 6(b), (c), and (d) show the steady state simulation results of PM1, PM2, and PM3 with two different sizes square shape initial conditions, respectively. We define steady state as a discrete l_2 norm (difference of ϕ^n and ϕ^{n+1}) becomes less than $tol = 1.0e-6$ which is a given tolerance. As shown in the top row numerical results of Fig. 6, when the initial shape is large enough, all three models work well. On the other hand, we obtain the results that the objects stay as shown in the bottom row of Fig. 6(c) and (d), which are results of PM2 and PM3, respectively. That is, when the object is small, in the case of PM1, the object disappears (see the bottom row of Fig. 6(b)). The reason why the small objects disappear is that in the case of PM1, a constant value is equally corrected over the entire area to conserve the mass, while PM2 and PM3 perform correction only around the interface, therefore, the phenomenon appears differently. Fig. 7 shows the change of the interface of PM1 over time when it has a small object as initial condition.

Fig. 8(a) and 9(a) show the maximum and minimum values of each model according to iteration for the different size of the initial object. It should be noted that the value of ϕ is 0.009 for PM1, however, the values are 0.0 for PM2 and PM3. In addition, it can be seen that the

PM1 does not satisfy the maximum principle. The reason is that the PM1 corrects the mass in the entire computational domain, but the PM2 and the PM3 are correct the mass only around the interface in Fig. 8(b) and Fig. 9(b).

From the results of Figs. 8 and 9, it can be seen that our proposed model PM3 satisfies the maximal principle and maintains its shape better than the PM1, especially when the initial object is small. There is a difference from the PM2 in the results of Figs. 8(b) and 9(b). This shows that the results of our proposed method are more accurate through the test of the radius, which changes with time when there are two initial circle shapes in the next Section 3.2.

Next, in Fig. 10, we show the numerical results of the two previous models and our proposed model when cubes of different sizes are used as initial shapes. The initial conditions are (1) when $40 \leq i, j, k \leq 88$, the value of ϕ_{ijk} is 1, (2) when $52 \leq i, j, k \leq 76$, the value of ϕ_{ijk} is 1, and otherwise the value of ϕ_{ijk} is 0, as shown in Fig. 10(a) for the isosurface $\phi = 0.5$ on $\Omega = [0, 1]^3$ with $h = 1/128$. We use $\Delta t = 1.0e-5$. Figs. 10(b), (c), and (d) show the results at steady state of PM1, PM2, and PM3, respectively. It can be seen that the 3D results are similar to the two-dimensional results.

In Fig. 11, we compare the cross-sections of the 3D numerical results of each model seen in Fig. 10. As with the 2D simulation results, it can be seen that the PM1 does not satisfy the maximum principle when the initial shape is large (Fig. 11(a)). Also, the PM1 could not maintain its shape compared with the PM2 and PM3 for a small initial shape (Fig. 11(b)).

As shown in Fig. 11, it can be seen that the PM2 satisfies the maximum principle but preserves the shape more than the PM3 when evolution proceeds to a steady state regardless of the initial shape size. In the next Section 3.2, we check the analytic radii of two circles over time to demonstrate our proposed method is more accurate.

3.2. Evolution of circles

The authors [49] computed the respective evolution laws for the interfaces explicitly in the radial case. When m circles(spheres) with radii r_i for $i = 1, 2, \dots, m$ and $r_j < r_{j+1}$ for $j = 1, 2, \dots, m - 1$ in n -dimensional space, the change in radii with time can be computed by the following equation

$$\frac{dr_i}{dt} = (n - 1) \left(\frac{\sum_{k=1}^m r_k^{n-2}}{\sum_{k=1}^m r_k^{n-1}} - \frac{1}{r_i} \right), \quad i = 1, 2, \dots, m. \quad (46)$$

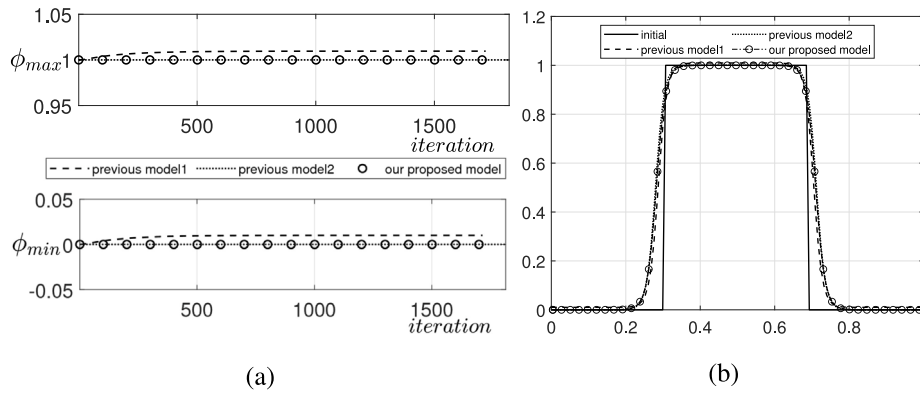


Fig. 8. (a) Maximum and minimum values of each model according to iterations and (b) interface comparison of numerical results of each model at initial and final time with large initial shapes.

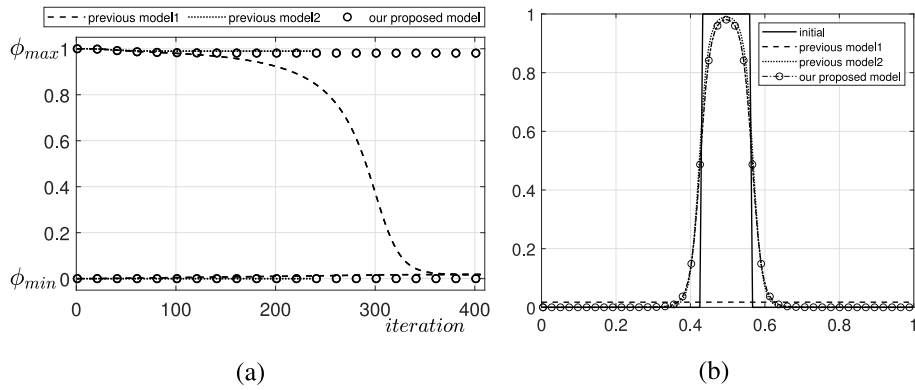


Fig. 9. (a) Maximum and minimum values of each model according to iterations and (b) interface comparison of numerical results of each model at initial and final time with small initial shapes.

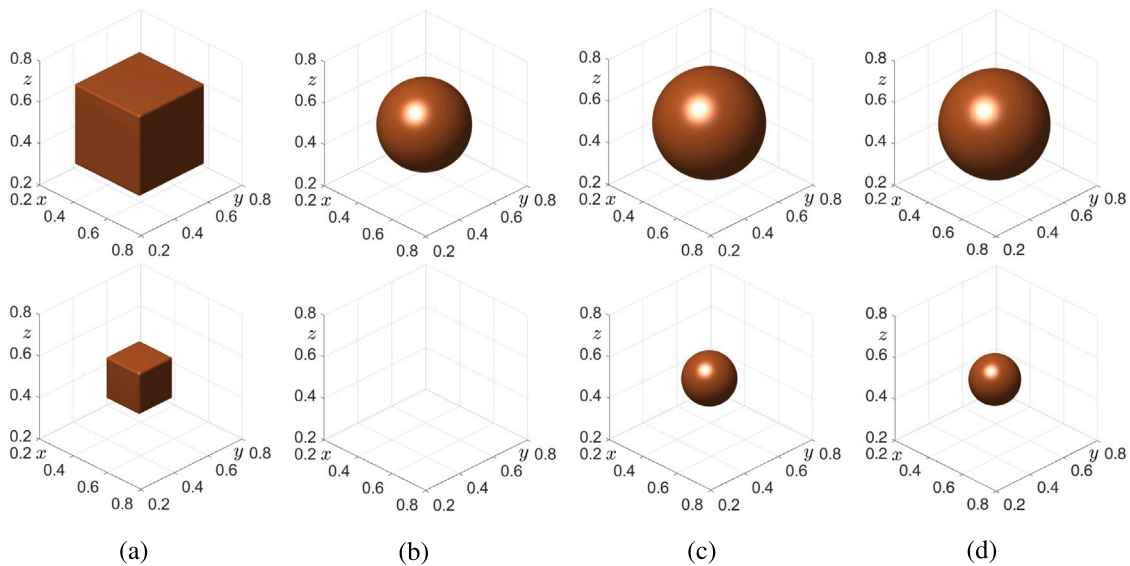


Fig. 10. (a): Initial cube shapes with different sizes. (b)–(d): The numerical results at steady state of PM1, PM2, and PM3, respectively.

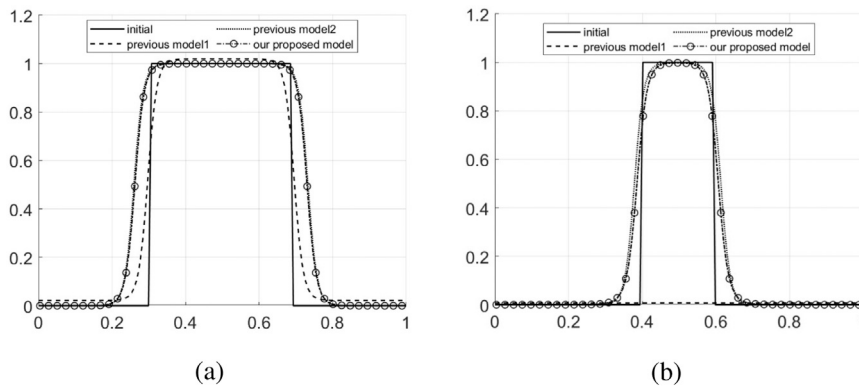


Fig. 11. Interface comparison of numerical results of each model at initial and final time with (a) large, and (b) small initial shapes.

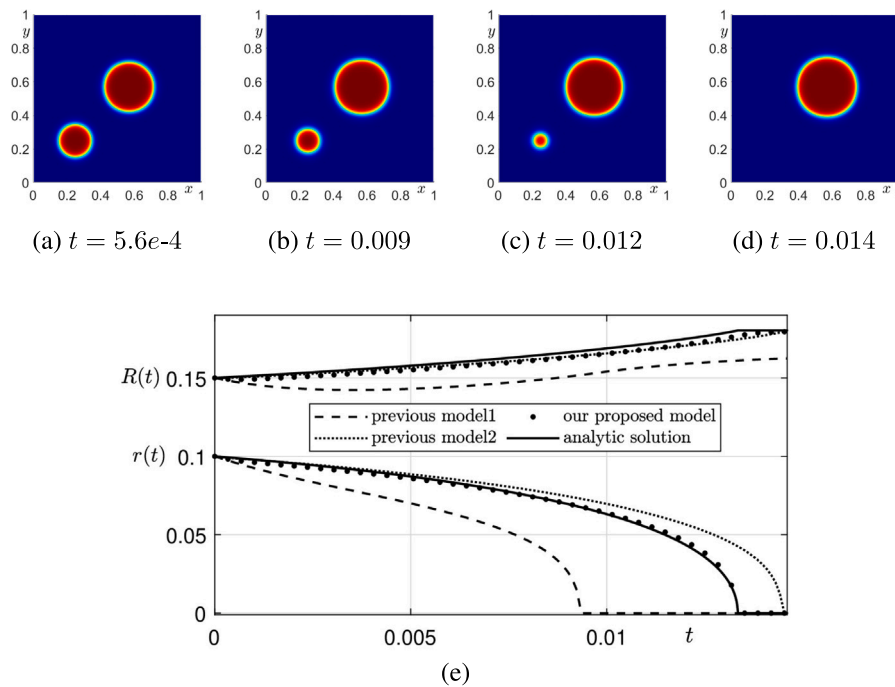


Fig. 12. The bottom result shows that the change of the radii (r and R) over time for PM1, PM2, PM3, and analytic solution. We present the analytic solution as the solid lines.

We take initial condition as two circle shapes with radii r and R (here, $r < R$) in two-dimensional space and measure the change in radii over time. From Eq. (46),

$$\frac{dr}{dt} = \frac{2}{r+R} - \frac{1}{r}, \quad \frac{dR}{dt} = \frac{2}{r+R} - \frac{1}{R}. \tag{47}$$

Using Eq. (47), we can obtain t_f which is the time when the small circle disappears [22]:

$$t_f = -0.5r_0R_0 + 0.25(r_0^2 + R_0^2) \ln\left(1 + \frac{2r_0R_0}{(R_0 - r_0)^2}\right), \tag{48}$$

where r_0 and R_0 are the initial radii of circles. We set the $r_0 = 0.1$, $R_0 = 0.15$, $\Delta t = 1.1264e-4$, $\Omega = [0.1]^2$ with 128×128 mesh grid. Then, from Eq. (48), we obtain the $t_f = 0.0133$. We numerically solve Eq. (46) using the 4th order RK method [45] to get the reference solution of radii (r and R).

Fig. 12 shows that PM3's results predict well the radii r and R along the analytic solution line. The results of PM1 do not match the analytic solution. It is because the Lagrangian multiplier acts on the entire interface. Therefore, most of the mass diffuses into the bulk phase. The results of the PM2 show that the shape of a small circle is more preserved compared to the analytic solution line.

3.3. Satisfying maximum principle and unconditional stability

In this section, we perform a numerical experiment to show that our proposed scheme has practically unconditional stability. We use random initial condition which has perturbation around 0.5 in Fig. 13(a):

$$\phi(x, y, 0) = 0.5 + 0.02\text{rand}(x, y), \tag{49}$$

here, $\text{rand}(x, y)$ is a random number in $[-1, 1]$. To show unconditional stability, we use different Δt as $0.01h^2$, h^2 , $10h^2$, and $100h^2$ on $\Omega = [0, 1]^2$ with uniform mesh 128^2 .

Figs. 13(b), (c), and (d) demonstrate that the proposed method is unconditionally stable. To get an accurate numerical approximation, the value of Δt is usually used less than $0.1h^2$. Otherwise, the numerical results can lead to large discretization errors. Therefore, we can use over 1,000 times larger time step than $\Delta t = 0.01h^2$, which indicates that our proposed method is unconditionally stable. In addition, the diffusion and reaction terms in the proposed algorithm was theoretically proved unconditionally stable in [43]. The term for mass conservation is also unconditionally stable by construction of the procedure, therefore, the entire step is unconditionally stable. Furthermore, it can be confirmed

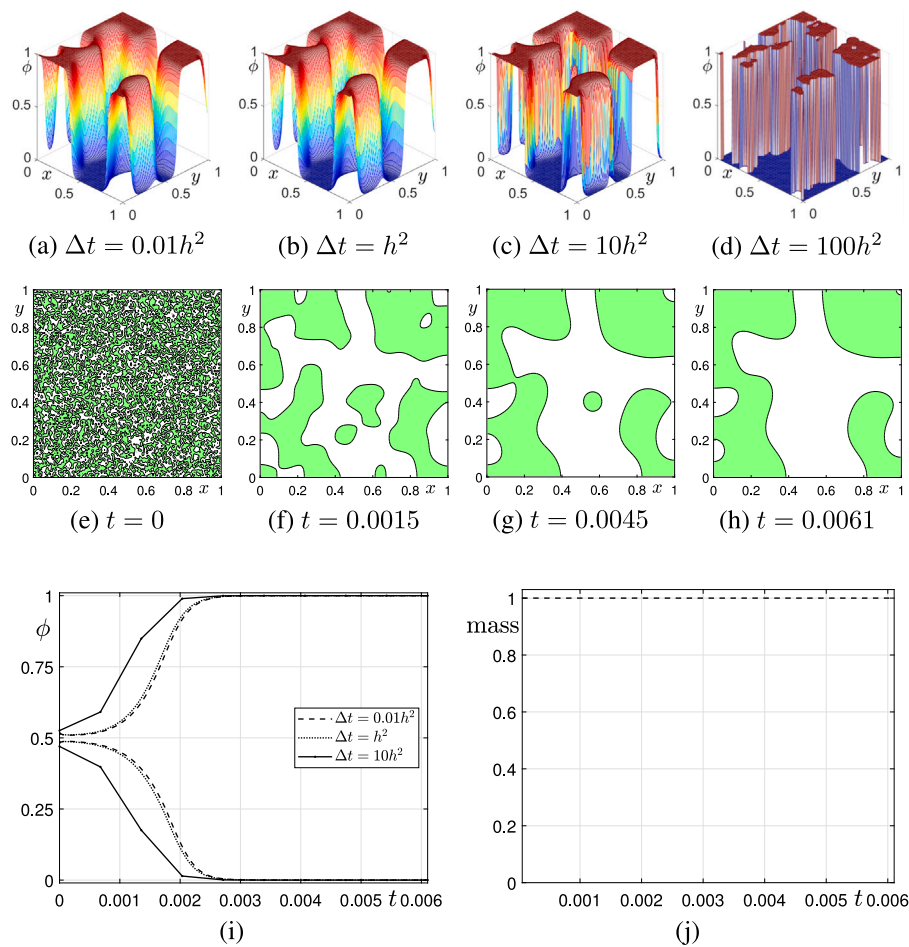


Fig. 13. (a)–(d) Evolution results at $T = 100h^2$ with four different Δt . (e)–(h) 0.5 level contour results for $\Delta t = h^2$ at each time. (i) The maximum and minimum values of ϕ versus time t . (j) The change in mass over time for $\Delta t = h^2$. The mass is defined as $\text{mass}(t)/\text{mass}(1)$, i.e., (j) is drawn by dividing the mass at each time by the initial mass.

that the maximum and minimum values with arbitrary Δt do not exceed 0 and 1 as shown in Fig. 13(e). Therefore, our proposed scheme has unconditional stability and satisfies the maximum principle.

4. Conclusions

In this paper, we presented a maximum principle preserving and unconditionally stable numerical method for the CAC equation. There have been many research works for the numerical methods for the CAC equation. To conserve the total mass, many methods introduced Lagrange multipliers which are added to the Allen–Cahn equation. Therefore, some of the methods do not preserve the maximum principle, i.e., it is possible to have values greater than one. In this paper, we proposed a new time-dependent Lagrange multiplier which is a power exponent to the concentration so that the maximum principle strictly holds. We described the proposed numerical algorithm in detail and presented several computational tests to demonstrate the superior performance of the scheme.

Declaration of competing interest

The authors declare that they have no known competing financial interests or personal relationships that could have appeared to influence the work reported in this paper.

Data availability

No data was used for the research described in the article.

Acknowledgments

The first author (Y. Choi) was supported by Basic Science Research Program through the National Research Foundation of Korea (NRF) funded by the Ministry of Education (2022R111A307282411). The corresponding author (J.S. Kim) was supported by the National Research Foundation of Korea (NRF) grant funded by the Korea government (MSIT) (No. 2022R1A2C1003844). The authors are grateful to the reviewers whose comments greatly improved the paper.

References

- [1] Allen SM, Cahn JW. A microscopic theory for antiphase boundary motion and its application to antiphase domain coarsening. *Acta Metall* 1979;27(6):1085–95.
- [2] Mohammadi V, Mirzaei D, Dehghan M. Numerical simulation and error estimation of the time-dependent Allen–Cahn equation on surfaces with radial basis functions. *J Sci Comp* 2019;79:493–516.
- [3] Tan Z, Zhang C. The discrete maximum principle and energy stability of a new second-order difference scheme for Allen–Cahn equations. *Appl Numer Math* 2021;166:227–37.
- [4] Hong Q, Gong Y, Zhao J, Wang Q. Arbitrarily high order structure-preserving algorithms for the Allen–Cahn model with a nonlocal constraint. *Appl Numer Math* 2021;170:321–39.
- [5] Du J, Chung E, Yang Y. Maximum-principle-preserving local discontinuous Galerkin methods for Allen–Cahn equations. *Comm Appl Math Comput* 2022;4(1):353–79.
- [6] Poochinapan K, Wongsaijai B. Numerical analysis for solving Allen–Cahn equation in 1D and 2D based on higher-order compact structure-preserving difference scheme. *Appl Math Comput* 2022;434:127374.
- [7] Lee C, Choi Y, Kim J. An explicit stable finite difference method for the Allen–Cahn equation. *Appl Numer Math* 2022;182:87–99.

- [8] Huang Z, Lin G, Ardekani AM. Consistent and conservative scheme for incompressible two-phase flows using the conservative Allen–Cahn model. *J Comput Phys* 2020;420:109718.
- [9] Ren F, Song B, Sukop MC, Hu H. Improved lattice Boltzmann modeling of binary flow based on the conservative Allen–Cahn equation. *Phys Rev E* 2016;94(2):023311.
- [10] Yang J, Jeong D, Kim J. A fast and practical adaptive finite difference method for the conservative Allen–Cahn model in two-phase flow system. *Int J Multiph Flow* 2021;137:103561.
- [11] Aihara S, Takaki T, Takada N. Multi-phase-field modeling using a conservative Allen–Cahn equation for multiphase flow. *Comput & Fluids* 2019;178:141–51.
- [12] Huang Z, Lin G, Ardekani AM. A consistent and conservative volume distribution algorithm and its applications to multiphase flows using phase-field models. *Int J Multiph Flow* 2021;142:103727.
- [13] Wu J, Yang J, Tan Z. Unconditionally energy-stable time-marching methods for the multi-phase conservative Allen–Cahn fluid models based on a modified SAV approach. *Comput Meth Appl Mech Eng* 2022;398:115291.
- [14] Kim J, Jeong D, Yang SD, Choi Y. A finite difference method for a conservative Allen–Cahn equation on non-flat surfaces. *J Comput Phys* 2017;334:170–81.
- [15] Yang J, Kim J. Numerical study of incompressible binary fluids on 3D curved surfaces based on the conservative Allen–Cahn–Navier–Stokes model. *Comput & Fluids* 2021;228:105094.
- [16] Geng S, Li T, Ye T, Yang X. A new conservative Allen–Cahn type Ohta–Kawaski phase-field model for diblock copolymers and its numerical approximations. *Adv Appl Math Mech* 2022;14(1):101–24.
- [17] Rubinstein J, Sternberg P. Nonlocal reaction–diffusion equations and nucleation. *IMA J Appl Math* 1992;48(3):249–64.
- [18] Okumura M. A stable and structure-preserving scheme for a non-local Allen–Cahn equation. *Jpn J Ind Appl Math* 2018;35(3):1245–81.
- [19] Wu J, Yang J, Tan Z. Unconditionally energy-stable time-marching methods for the multi-phase conservative Allen–Cahn fluid models based on a modified SAV approach. *Comput Meth Appl Mech Eng* 2022;398:115291.
- [20] Lee HG, Shin J, Lee JY. A high-order and unconditionally energy stable scheme for the conservative Allen–Cahn equation with a nonlocal Lagrange multiplier. *J Sci Comput* 2022;90(1):1–12.
- [21] Zhang Z, Tang H. An adaptive phase field method for the mixture of two incompressible fluids. *Comput & Fluids* 2007;36(8):1307–18.
- [22] Brassel M, Bretin E. A modified phase field approximation for mean curvature flow with conservation of the volume. *Math Methods Appl Sci* 2011;10(34):1157–80.
- [23] Lee HG. High-order and mass conservative methods for the conservative Allen–Cahn equation. *Comput Math Appl* 2016;72(3):620–31.
- [24] Jiang K, Ju L, Li J, Li X. Unconditionally stable exponential time differencing schemes for the mass-conserving Allen–Cahn equation with nonlocal and local effects. *Numer Meth Part Differ Equ* 2021.
- [25] Kim J, Lee S, Choi Y. A conservative Allen–Cahn equation with a space–time dependent Lagrange multiplier. *Int J Eng Sci* 2014;84:11–7.
- [26] Chai Z, Sun D, Wang H, Shi B. A comparative study of local and nonlocal Allen–Cahn equations with mass conservation. *Int J Heat Mass Transf* 2018;122:631–42.
- [27] Kwak S, Yang J, Kim J. A conservative Allen–Cahn equation with a curvature-dependent Lagrange multiplier. *Appl Math Lett* 2022;126:107838.
- [28] Dehghan M, Mohammadi V. The numerical simulation of the phase field crystal (PFC) and modified phase field crystal (MPFC) models via global and local meshless methods. *Comput Methods Appl Mech Engrg* 2016;298:453–84.
- [29] Choi Y, Jeong D, Kim J. A multigrid solution for the Cahn–Hilliard equation on nonuniform grids. *Appl Math Comput* 2017;293:320–33.
- [30] Dehghan M, Abbaszadeh M. The meshless local collocation method for solving multi-dimensional Cahn–Hilliard, Swift–Hohenberg and phase field crystal equations. *Eng Anal Bound Elem* 2017;78:49–64.
- [31] Jeong D, Choi Y, Kim J. A benchmark problem for the two-and three-dimensional Cahn–Hilliard equations. *Commun Nonlinear Sci Numer Simul* 2018;61:149–59.
- [32] Mohammadi V, Dehghan M. Simulation of the phase field Cahn–Hilliard and Tumor growth models via a numerical scheme: Element-free Galerkin method. *Comput Methods Appl Mech Engrg* 2019;345:919–50.
- [33] Mohammadi V, Dehghan M. A meshless technique based on generalized moving least squares combined with the second-order semi-implicit backward differential formula for numerically solving time-dependent phase field models on the spheres. *Appl Numer Math* 2020;153:248–75.
- [34] Dehghan M, Gharibi Z. Numerical analysis of fully discrete energy stable weak Galerkin finite element scheme for a coupled Cahn–Hilliard–Navier–Stokes phase-field model. *Appl Math Comput* 2021;410:126487.
- [35] Kim Y, Choi Y. Learning finite difference methods for reaction–diffusion type equations with FCNN. *Comput Math Appl* 2022;123:115–22.
- [36] Ju L, Li X, Qiao Z, Yang J. Maximum bound principle preserving integrating factor Runge–Kutta methods for semilinear parabolic equations. *J Comput Phys* 2021;439:110405.
- [37] Zhang H, Yan J, Qian X, Chen X, Song S. Explicit third-order unconditionally structure-preserving schemes for conservative Allen–Cahn equations. *J Sci Comput* 2022;90(1):1–29.
- [38] Weng Z, Zhuang Q. Numerical approximation of the conservative Allen–Cahn equation by operator splitting method. *Math Methods Appl Sci* 2017;40(12):4462–80.
- [39] Lee HG, Lee JY. A second order operator splitting method for Allen–Cahn type equations with nonlinear source terms. *Physica A* 2015;432:24–34.
- [40] Mazloum J, Siahal-Mahalle BH. An efficient operator-splitting radial basis function-generated finite difference (RBF-FD) scheme for image noise removal based on nonlinear total variation models. *Eng Anal Bound Elem* 2022;143:740–54.
- [41] Li D, Quan C, Xu J. Stability and convergence of strang splitting. Part I: Scalar Allen–Cahn equation. *J Comput Phys* 2022;458:111087.
- [42] Li D, Quan C, Xu J. Stability and convergence of strang splitting. Part II: Tensorial Allen–Cahn equations. *J Comput Phys* 2022;454:110985.
- [43] Lee S. Non-iterative compact operator splitting scheme for Allen–Cahn equation. *Comput Appl Math* 2021;40(7):1–9.
- [44] Lee HG, Kim J. Accurate contact angle boundary conditions for the Cahn–Hilliard equations. *Comput & Fluids* 2011;44(1):178–86.
- [45] Faires JD, Burden RL. Numerical methods. 4th ed.. Cengage Learning; 2012.
- [46] Wu C, Feng X, He Y, Qian L. A second-order strang splitting scheme with exponential integrating factor for the Allen–Cahn equation with logarithmic Flory–Huggins potential. *Commun Nonlinear Sci Numer Simul* 2023;117:106983.
- [47] Park J, Lee C, Choi Y, Lee HG, Kwak S, Hwang Y, et al. An unconditionally stable splitting method for the Allen–Cahn equation with logarithmic free energy. *J Eng Math* 2022;132(1):1–18.
- [48] Kim J. Phase-field models for multi-component fluid flows. *Commun Comput Phys* 2012;12(3):613–61.
- [49] Bronsard L, Stoth B. Volume-preserving mean curvature flow as a limit of a nonlocal Ginzburg–Landau equation. *SIAM J Math Anal* 1997;28(4):769–807.